Supplementary Information for: The Case Against Hole Injection Through SAMs in Perovskite Solar Cells

Fraser J. Angus[1†], Lewis Mackenzie[1†], Marcin Giza[1], Dylan Wilkinson[1], Elisabetta Arca[2], Emilio Palomares[3,4], Wenhui Li[3], Pablo Docampo[1,5]*, Graeme Cooke[1]**

[1]School of Chemistry, University of Glasgow, Glasgow G12 8QQ, UK

[2]School of Mathematics, Statistics and Physics, Newcastle University, Newcastle upon Tyne, NE1 7RU, UK

[3]Institute of Chemical Research of Catalonia (ICIQ- CERCA), 43007 Tarragona, Spain

[4]Catalan Institution for Research and Advanced Studies (ICREA), 08010 Barcelona, Spain

[5]Basque Center for Materials, Applications and Nanostructures (BCMaterials), 48940 Leioa, Spain

[†]Authors contributed equally

[*]Graeme.Cooke@glasgow.ac.uk; Pablo.Docampo@bcmaterials.net; wli@iciq.es

Contents

Supplementary Note 1 – Spiro-B Synthesis & Characterisation.....2
Supplementary Note 2 – TRPL Analysis.....16
Supplementary Figures.....17
Supplementary Tables.....23

Supplementary Note 1 – Spiro-B Synthesis & Characterisation

A Bruker Avance III 400 spectrometer was used to obtain NMR spectra (^{1}H NMR at 400 MHz and ^{13}C NMR at 100 MHz) with chemical shift values given in ppm with reference to tetramethylsilane, and these were analysed using MestReNova®. The spin coupling patterns observed in NMR spectra are described as singlet (s), doublet (d), triplet (t), quartet (q), quintet (quint), multiplet (m) or a combination of these. Mass spectrometry was performed by the mass spectrometry service at the University of Glasgow (ESI). Melting points were recorded on an SMP-10 Stuart Scientific melting point machine and are uncorrected.

Merck silica gel 60 covered aluminium plates F254 were used for thin-layer chromatography (TLC) analysis. Column chromatography purification was carried out using silica gel (Fluorochem®) 40–63 nm 60 Å. Reagents were purchased from Sigma Aldrich®, Alfa Aesar ®, Fluorochem®, or BLD Pharm® and were used without further purification. Anhydrous solvents were obtained using an Innovative Technology Inc. Pure Solv 400-5-MD solvent purification system or purchased from Sigma Aldrich®.

Computational structural optimisations were performed using Gaussian 09, Revision D.01, 2013 and structures/molecular orbitals graphics were generated using GaussView 5.0.9. All structures were first optimised using the semi-empirical method AM1 and then optimised using B3LYP/3-

21G. Frequency calculations were performed on each structure to confirm a local minimum had been reached by the absence of imaginary frequencies.

The thermogravimetric analysis (TGA) was performed on a TA Instruments TGA 5500 using a platinum pan, with the temperature ranging from 30 °C to 600 °C at a rate of 10 °C/min. The differential scanning calorimetry (DSC) was run under N_2 on a TA Instruments DSC 25 using an aluminium pan. The sample was heated at a rate of 10 °C/min.

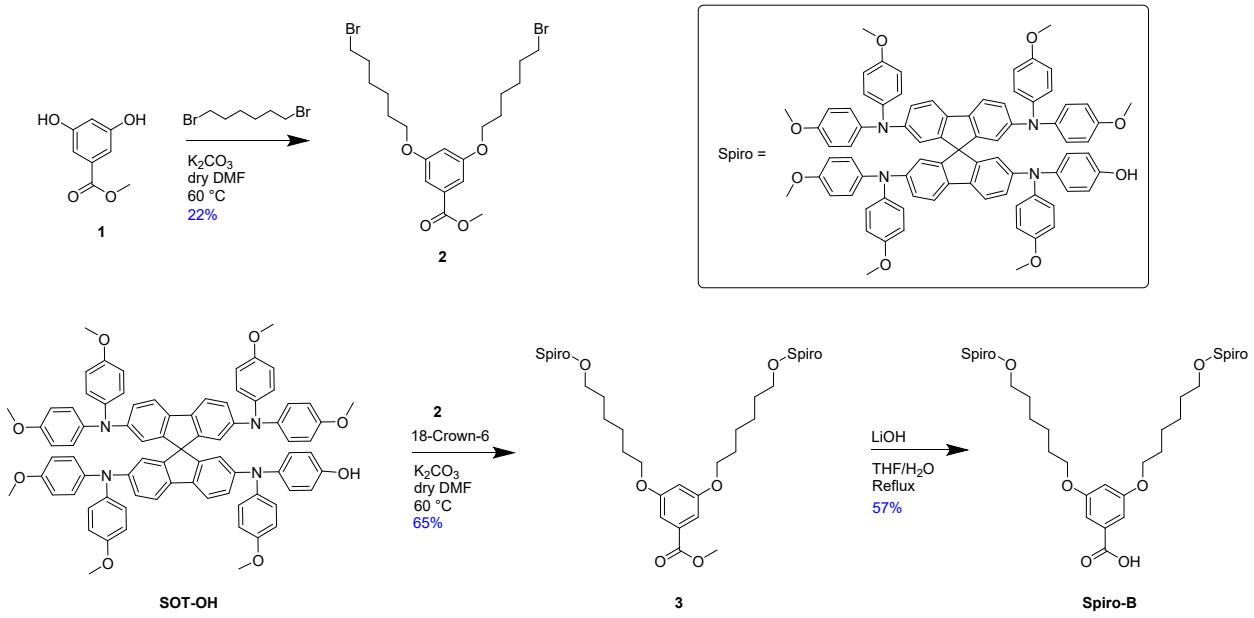

Scheme S1 Synthesis of **Spiro-B.**

Compound **2**[1]

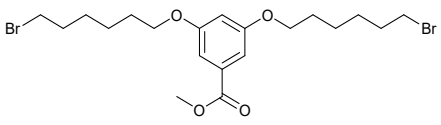

Compound **1** (1.00 g, 5.95 mmol) and potassium carbonate (2.47 g, 17.8 mmol) were dissolved in anhydrous dimethylformamide (25 mL), and the reaction was stirred at 60 °C under a nitrogen

atmosphere for 15 minutes. 1,6-Dibromohexane (7.25 g, 29.7 mmol) was then added. The reaction was stirred for 19 h before being poured into water (100 mL) and extracted with ethyl acetate (3 x 50 mL). The organic extracts were combined, washed with brine (100 mL), dried with magnesium sulphate, filtered, and the solvent removed under reduced pressure. The resulting residue was purified using silica gel chromatography (10% ethyl acetate in pet. ether) to give a clear oil (1.29 g). The product was further purified by dissolving it in a minimum volume of dichloromethane and then pouring it into petroleum ether (*ca.* 100 mL). After being left in a freezer (-18 °C) overnight, a precipitate formed, which was filtered and washed with petroleum ether to afford the title compound as a white crystalline powder (0.639 g, 21.7%). Mpt. 25–26 °C. ^{1}H NMR (400 MHz, $CDCl_3$) δ 7.16 (d, J = 2.3 Hz, 2H), 6.63 (t, J = 2.4 Hz, 1H), 3.98 (t, J = 6.4 Hz, 4H), 3.90 (s, 3H), 3.43 (t, J = 6.8 Hz, 4H), 1.89 (p, J = 6.9 Hz, 4H), 1.80 (p, J = 6.7 Hz, 4H), 1.58 – 1.43 (m, 8H). ^{13}C NMR (101 MHz, $CDCl_3$) δ 167.1, 160.2, 132.1, 107.8, 106.7, 68.2, 52.4, 33.9, 32.8, 29.1, 28.0, 25.4. HRMS *m/z* (ESI): [M+H$^+$] = 495.0568 ($C_{20}H_{31}Br_2O_4$ requires 495.0569). ν_{max}/cm^{-1} (neat) 2938 (*ar* C-H), 2859 (*alk* C-H), 1718 (C=O), 1592 (*ar* C=C), 1447 (*ar* C=C), 1435 (*ar* C=C), 1233 (*ar* C-O), 1161 (*ester* C=O), 1052 (*alk* C-O), 1013 (*alk* C-O).

Compound **3**

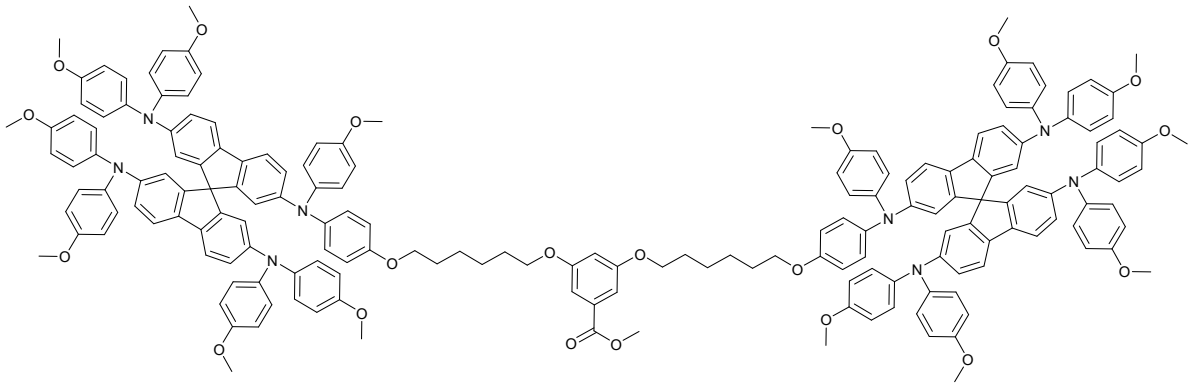

Compound **2** (0.060 g, 0.121 mmol), **SOT-OH** (0.309 g, 0.255 mmol), potassium carbonate (0.0671 g, 0.486 mmol), and a spatula tip of 18-crown-6 (*c.a.* 5 mg) were dissolved in anhydrous dimethylformamide (15 mL). The reaction was heated to 60 °C and stirred for 23 h. under a nitrogen atmosphere before being poured into water (150 mL), and the product was extracted with ethyl acetate (3 × 50 mL). The organic extracts were combined, washed with brine (50 mL), dried with magnesium sulphate, filtered, and solvent removed under reduced pressure. The resulting residue was purified using silica gel chromatography (4:4:1 petroleum ether: ethyl acetate: toluene) to give the title compound as an off-white solid (0.216 g, 64.7%). Mpt. 152 – 155 °C. ^{1}H NMR (400 MHz, C_6D_6) δ 7.59 (d, *J* = 2.3 Hz, 2H), 7.15 – 7.13 (m, 8H), 7.10 – 6.97 (m, 48H), 6.85 (t, *J* = 2.3 Hz, 1H), 6.84 – 6.81 (m, 4H), 6.77 – 6.72 (m, 28H), 3.63 (t, *J* = 6.4 Hz, 4H), 3.59 (t, *J* = 6.4 Hz, 4H), 3.29 – 3.25 (m, 42H), 1.60 – 1.49 (m, 8H), 1.31 – 1.20 (m, 8H). ^{13}C NMR (101 MHz, C_6D_6) δ 166.8, 161.0, 156.0, 156.0, 155.5, 150.9, 148.2, 142.0, 142.0, 135.9, 132.9, 125.9, 125.8, 123.0, 120.7, 118.4, 115.5, 115.0, 108.2, 107.2, 68.2, 68.0, 66.5, 55.0, 51.8, 29.6, 29.4, 26.1, 26.1. HRMS *m/z* (ESI): $[M]^{2+}$ = 1377.5898 ($C_{180}H_{159}N_8O_{20}$ requires 1377.5902). ν_{max}/cm^{-1} (neat) 3037 (*alk* C-H), 2903 (*alk* C-H), 2834 (*alk* C-H), 1722 (C=O), 1604 (*ar* C=C), 1504 (*ar* C=C), 1463 (*ar* C=C), 1237 (*ester/ar* C-O), 1034 (*alk* C-O).

Spiro-B

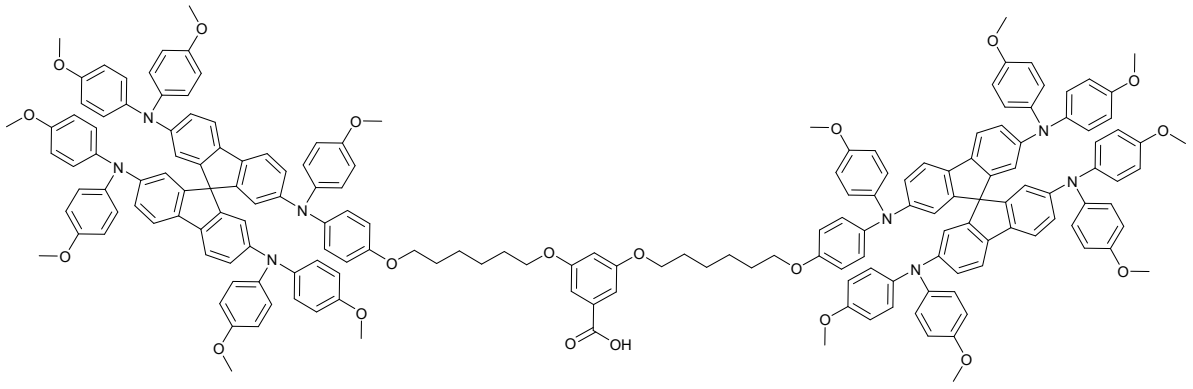

Compound **2** (0.100 g, 0.0363 mmol) was dissolved in tetrahydrofuran (10 mL), and then lithium hydroxide (6.55 mg, 0.273 mmol) dissolved in deionised water (0.5 mL) was added dropwise. The reaction was heated under reflux and stirred for 19.5 h under a nitrogen atmosphere before being cooled to room temperature. Aqueous hydrochloric acid (5% V/V) was then added dropwise until pH > 1 was achieved. The mixture was diluted with water (10 mL) and extracted with ethyl acetate (3 × 30 mL). The organic extracts were combined, washed with brine (2 x 60 mL), dried with magnesium sulphate, filtered, and solvent removed under reduced pressure. The resulting residue was dissolved in a minimum volume of ethyl acetate and poured dropwise into petroleum ether (*ca.* 60 mL). The precipitate was collected by filtration to afford the title compound as a white solid (0.057 g, 57.3%). Mpt. 168 – 171 °C. ^{1}H NMR (400 MHz, C_6D_6) δ 7.59 (d, *J* = 2.4 Hz, 2H), 7.17 – 7.12 (m, 6H), 7.12 – 6.94 (m, 48H), 6.86 (t, *J* = 2.3 Hz, 1H), 6.83 (d, *J* = 9.0 Hz, 4H), 6.74 (d, *J* = 9.0 Hz, 26H), 3.60 (t, *J* = 6.4 Hz, 8H), 3.34 – 3.23 (m, 42H), 1.60 – 1.49 (m, 8H), 1.29 – 1.21 (m, 8H). ^{13}C NMR (101 MHz, C_6D_6) δ 160.6, 155.6, 155.6, 155.1, 150.5, 147.8, 141.7, 141.6, 135.6, 135.5, 135.5, 125.6, 125.5, 122.6, 120.3, 117.9, 117.9, 115.2, 114.6, 108.2, 107.7, 67.8, 67.6, 66.2, 54.6, 29.3, 29.0, 25.8, 25.7. HRMS *m/z* (ESI): [M+H$^+$] = 2742.1703 ($C_{179}H_{159}N_8O_{20}$ requires 2742.1731). ν_{max}/cm^{-1} (neat) 3034 (*ar* C-H), 2904 (*alk* C-H), 2832 (*alk* C-H), 1726 (C=O), 1695 (C=O), 1605 (*ar* C=C), 1502 (*ar* C=C), 1461 (*ar* C=C), 1236 (*ester/ar* C-O), 1032 (*alk* C-O).

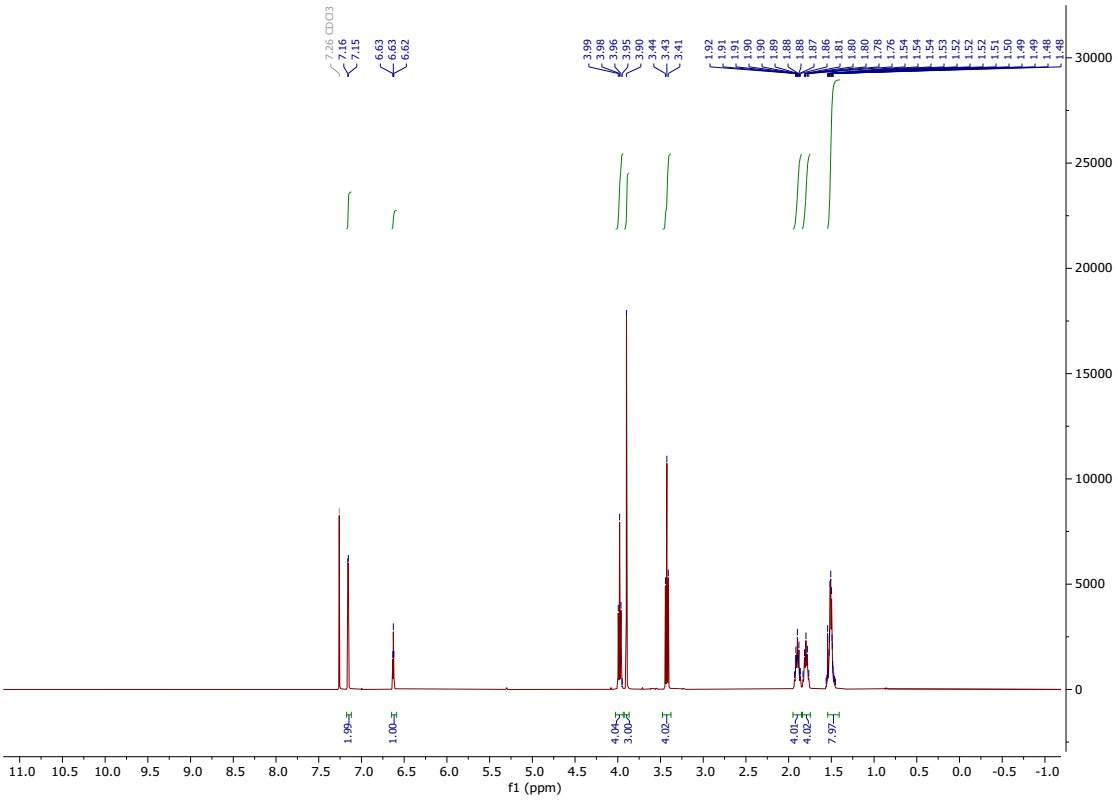

103

104 **Figure S1.** ^{1}H NMR of compound **2** in $CDCl_3$

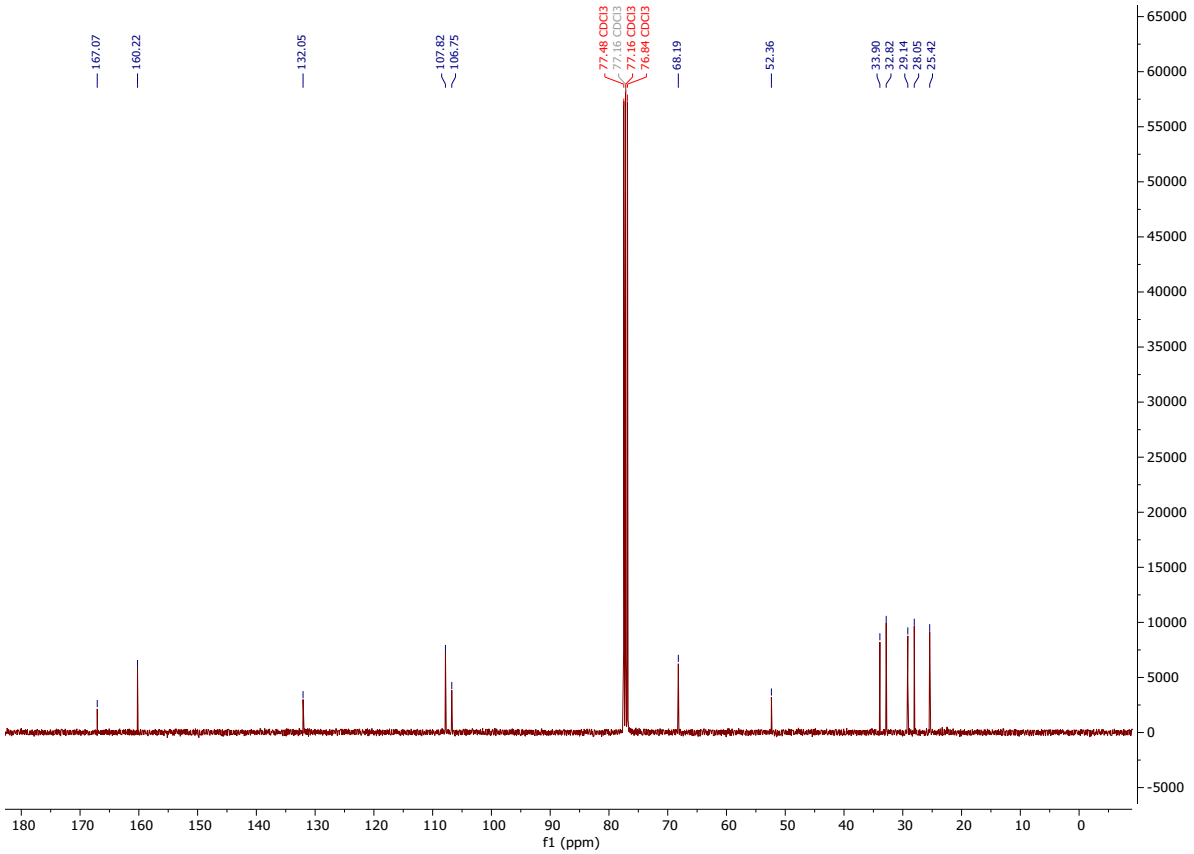

105

106 **Figure S2.** ^{13}C NMR of compound **2** in $CDCl_3$

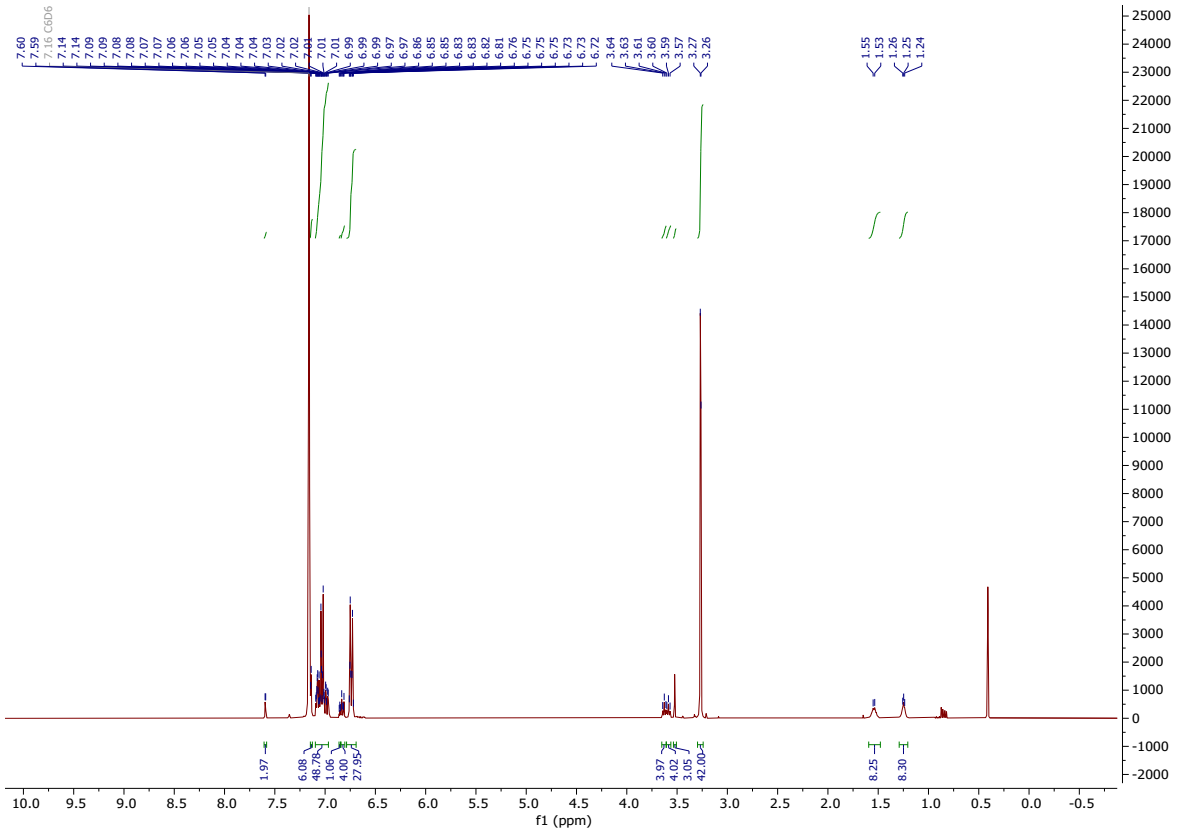

107

108 **Figure S3**. ^{1}H NMR of compound **3** C_6D_6

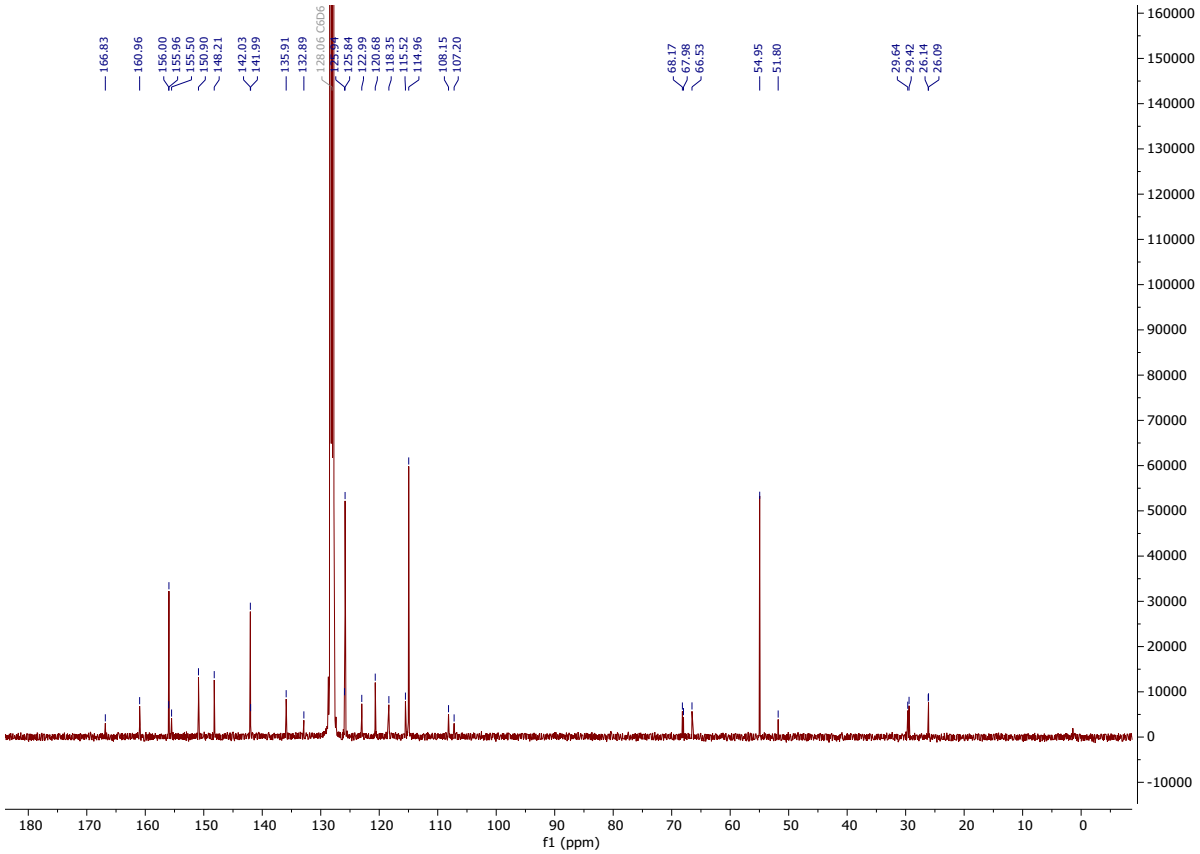

Figure S4. ^{13}C NMR of Compound **3** in C_6D_6

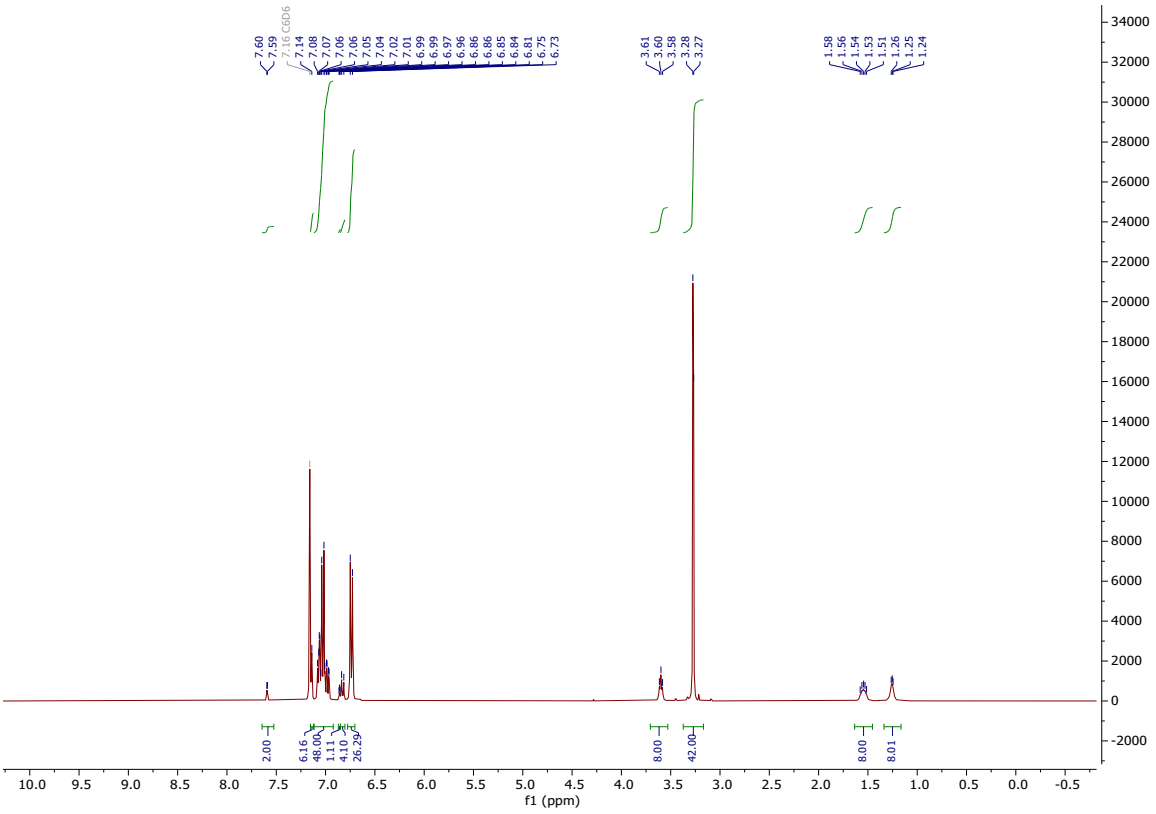

111

112 **Figure S5.** ^{1}H NMR **of Spiro-B** in C_6D_6

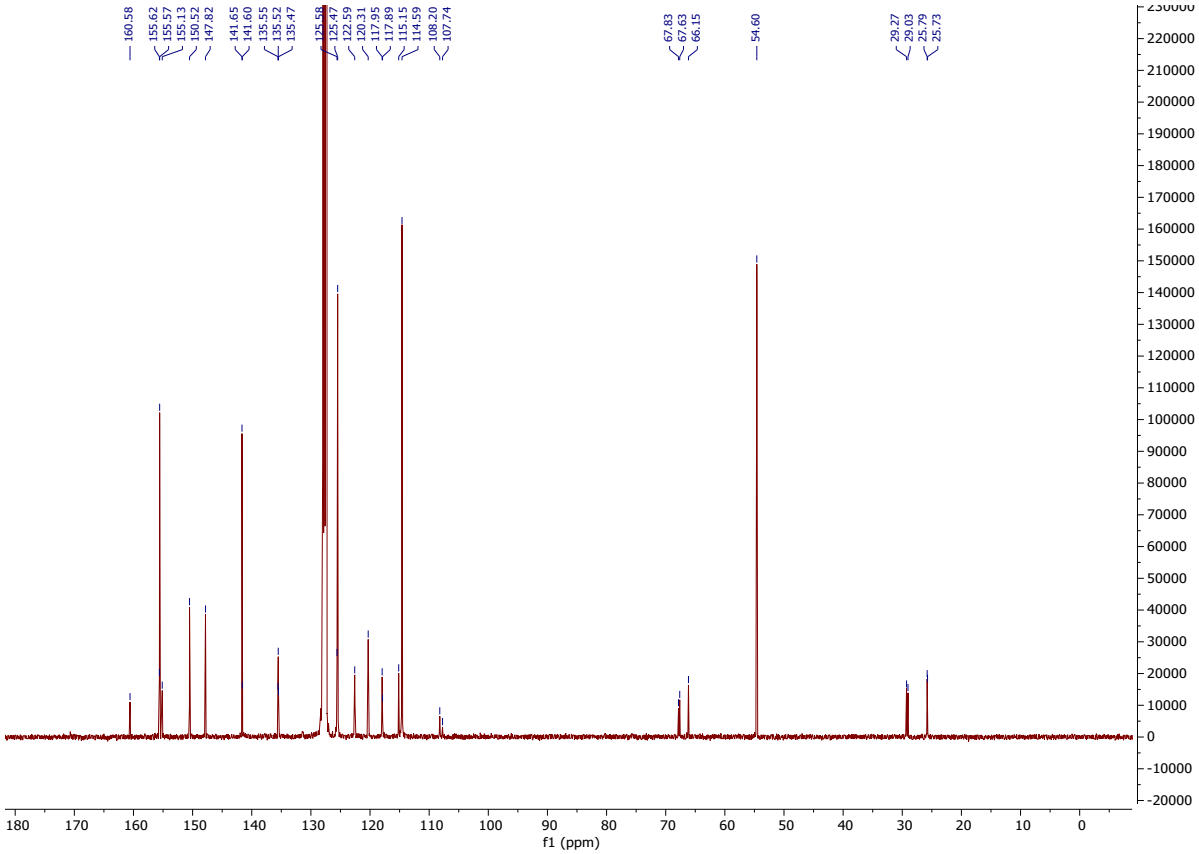

113

114 **Figure S6.** ^{13}C NMR of **Spiro-B** in C_6D_6

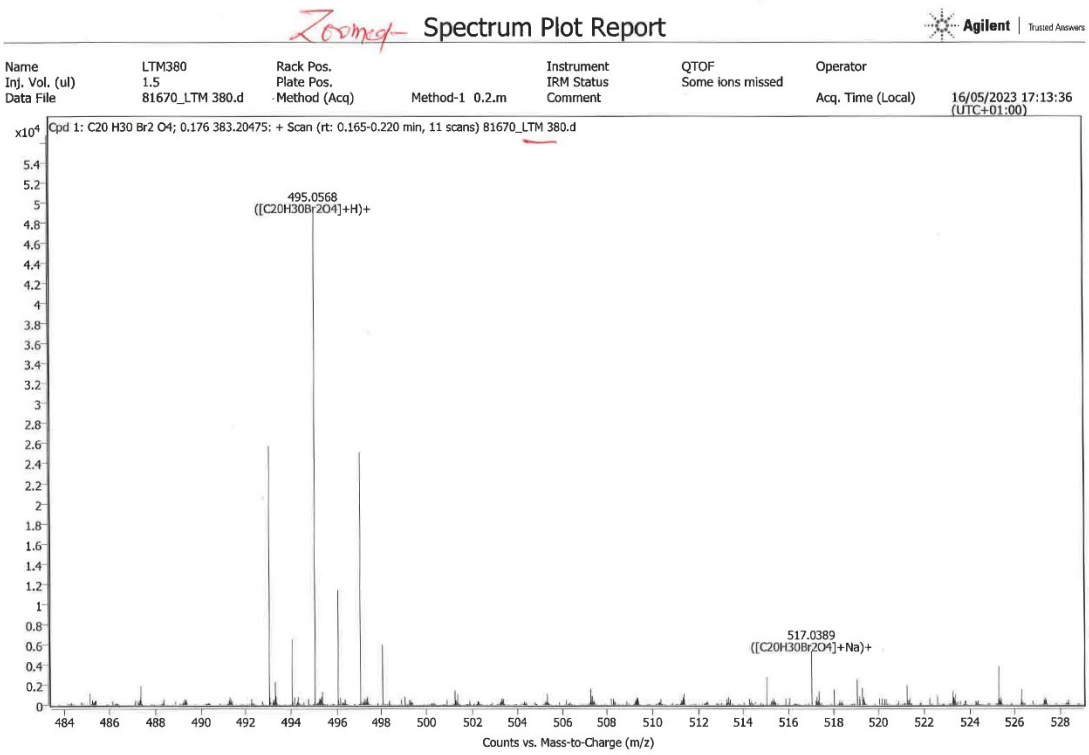

115 **Figure S7.** MS of compound **2**

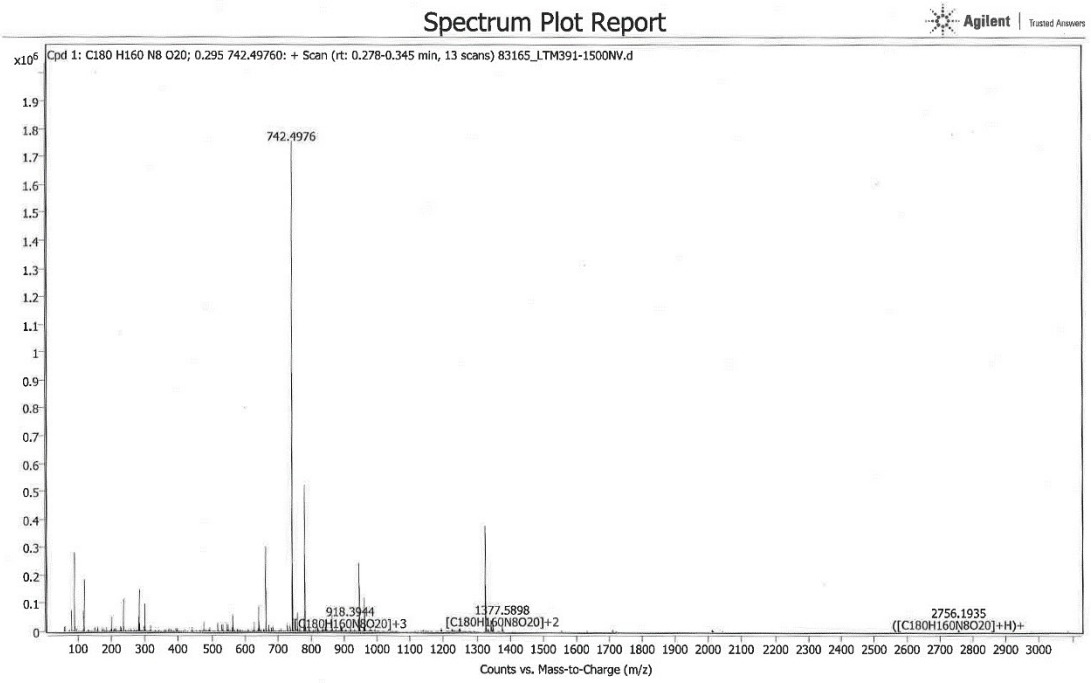

117

118 **Figure S8**. MS of compound **3**

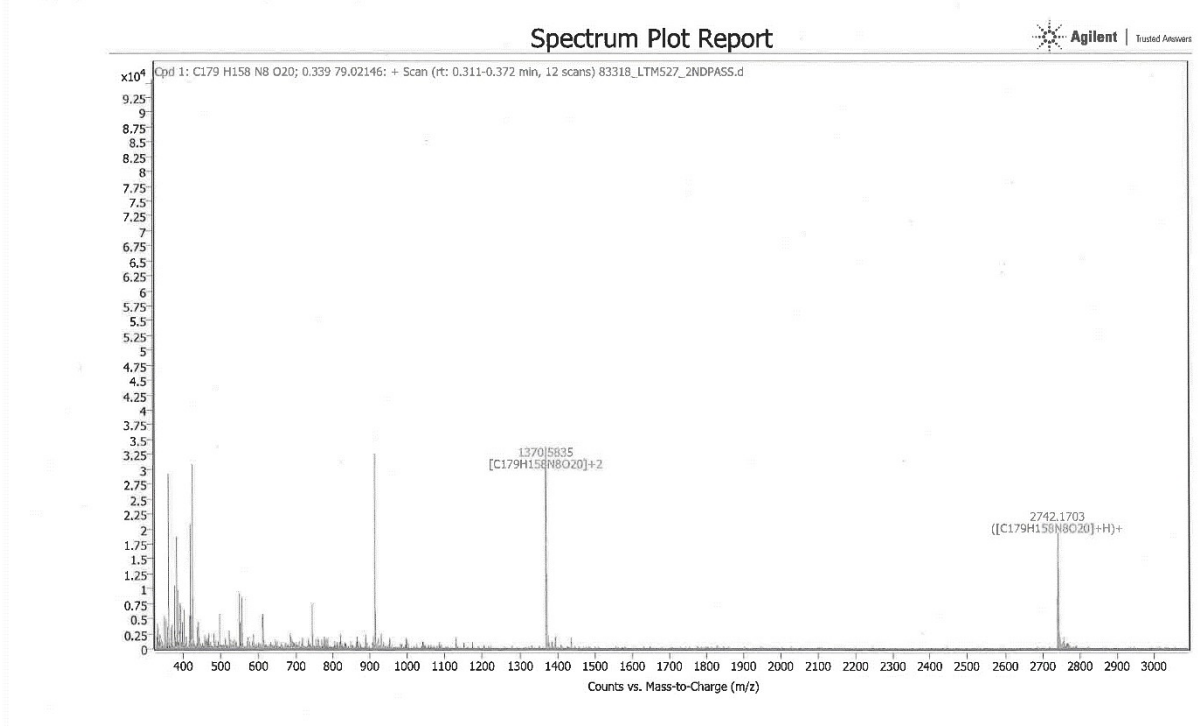

119

120 **Figure S9**. MS of compound **Spiro-B**

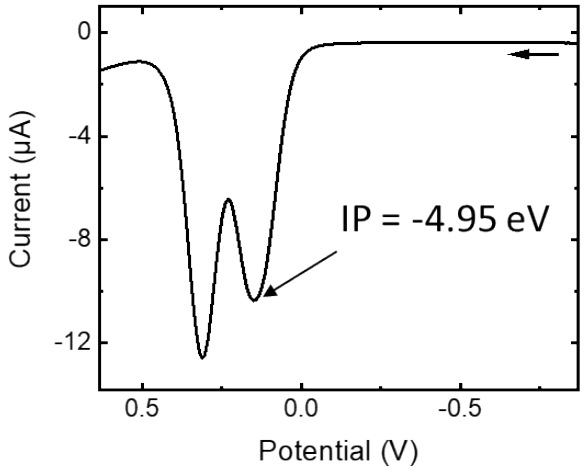

121

Figure S10. Square wave voltammetry of **Spiro-B** recorded in dichloromethane at a concentration of 10^{-4} mol L^{-1} and referenced to a ferrocenium/ferrocene standard. Direction of scan indicated on plot. Ionisation potential (IP) estimated as -4.80 eV (Fc^{+}/Fc) - 1st oxidation potential.

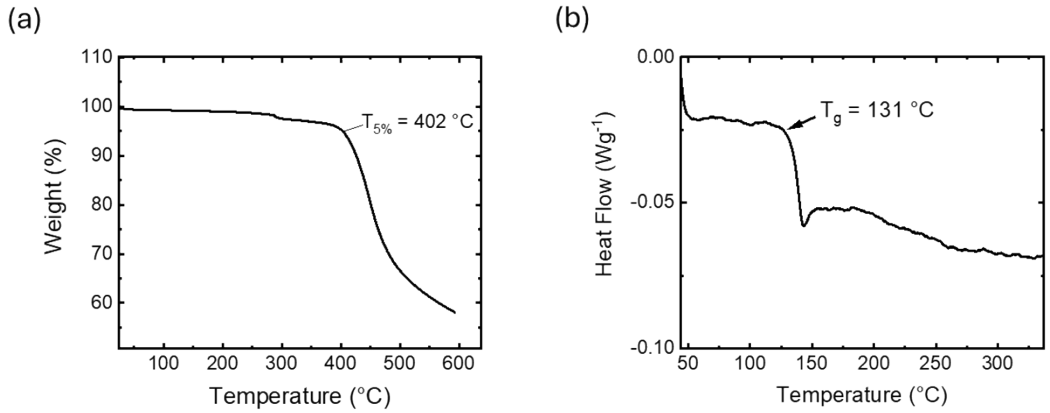

Figure S11. (a) TGA of **Spiro-B** T5% indicates the temperature at which a 5% weight loss is recorded. (b) DSC analysis of **Spiro-B**. A glass transition is noted at T = Tg.

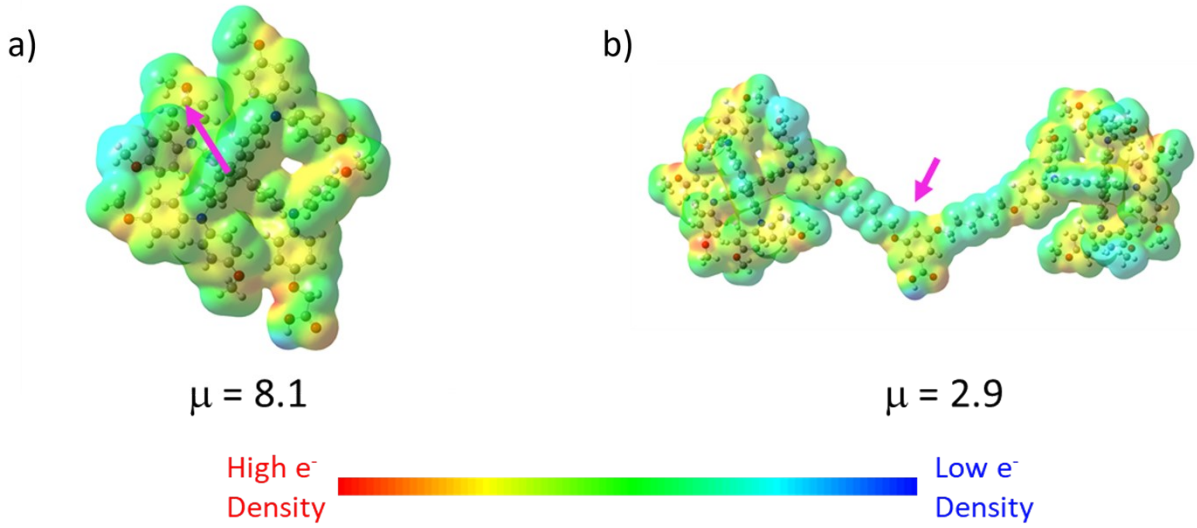

Figure S12. DFT B3LYP 3-21G optimised structures,[2] of (a) **Spiro-A** and (b) **Spiro-B** with ESP maps, dipole moment vector (indicated with a pink arrow pointing towards the positive pole), and dipole moment magnitudes shown below the structures.

Supplementary Note 2 – TRPL Analysis

To analyse the time-resolved photoluminescence (TRPL) decay of the perovskite films, we employed a rate equation model that accounts for dominant recombination pathways. The model describes the time-dependent carrier concentration n(t) using the differential equation **1**:

$$\frac{dn}{dt} = -k_1 n(t) - k_2 n^2(t) \quad \textbf{(1)}$$

where k_1 is the first-order (trap-assisted) recombination rate constant, and k_2 is the second-order (bimolecular) radiative recombination rate constant. To extract meaningful and literature-consistent values, we assume an initial photoexcited carrier concentration of $n_0 = 1.0\times10^{15}$ cm^{-3}, as this value was not obtained at the time of the measurement. The resulting values extracted from applying the rate equation can be seen in **Supplementary Table S2**.

Supplementary Figures

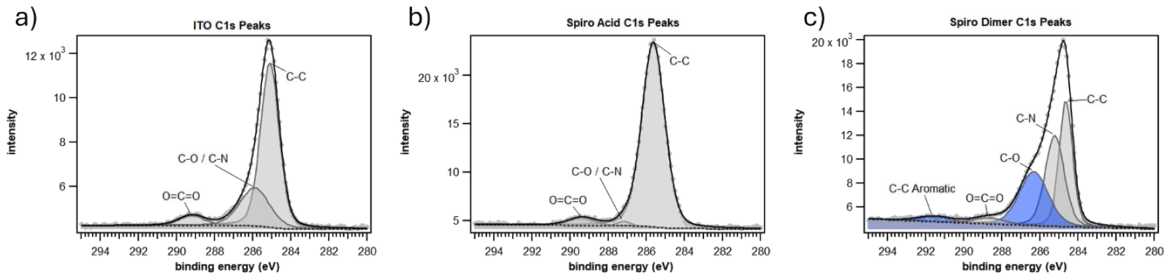

Figure S13. C1s XPS spectra of a) an ITO substrate, b) ITO coated with **Spiro-A**, c) ITO coated with **Spiro-B**.

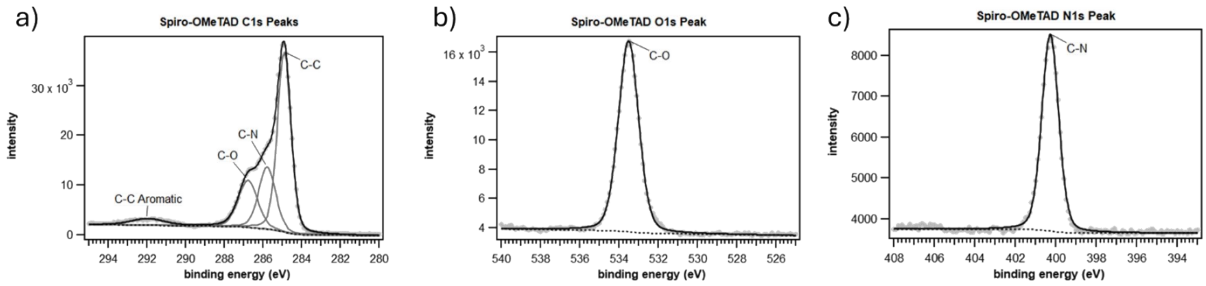

Figure S14. High-resolution XPS spectra of the a) C1s, b) O1s, and c) N1s regions of a thin film of spin-coated Spiro-OMeTAD.

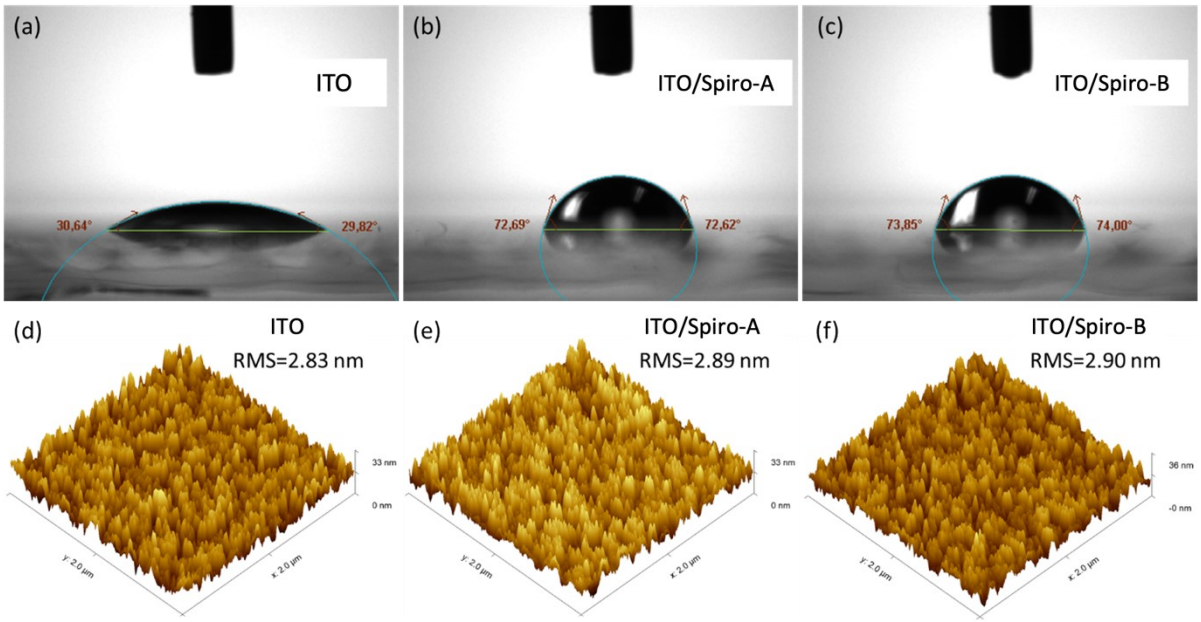

151

152 **Figure S15.** Contact angle measurements of water droplet on a) ITO, b) **Spiro-A**, and c) **Spiro-B**.

153 Atomic force microscopy (AFM) images of d) ITO, e) **Spiro-A**, and f) **Spiro-B**. Here, RMS is the

154 root-mean-square roughness.

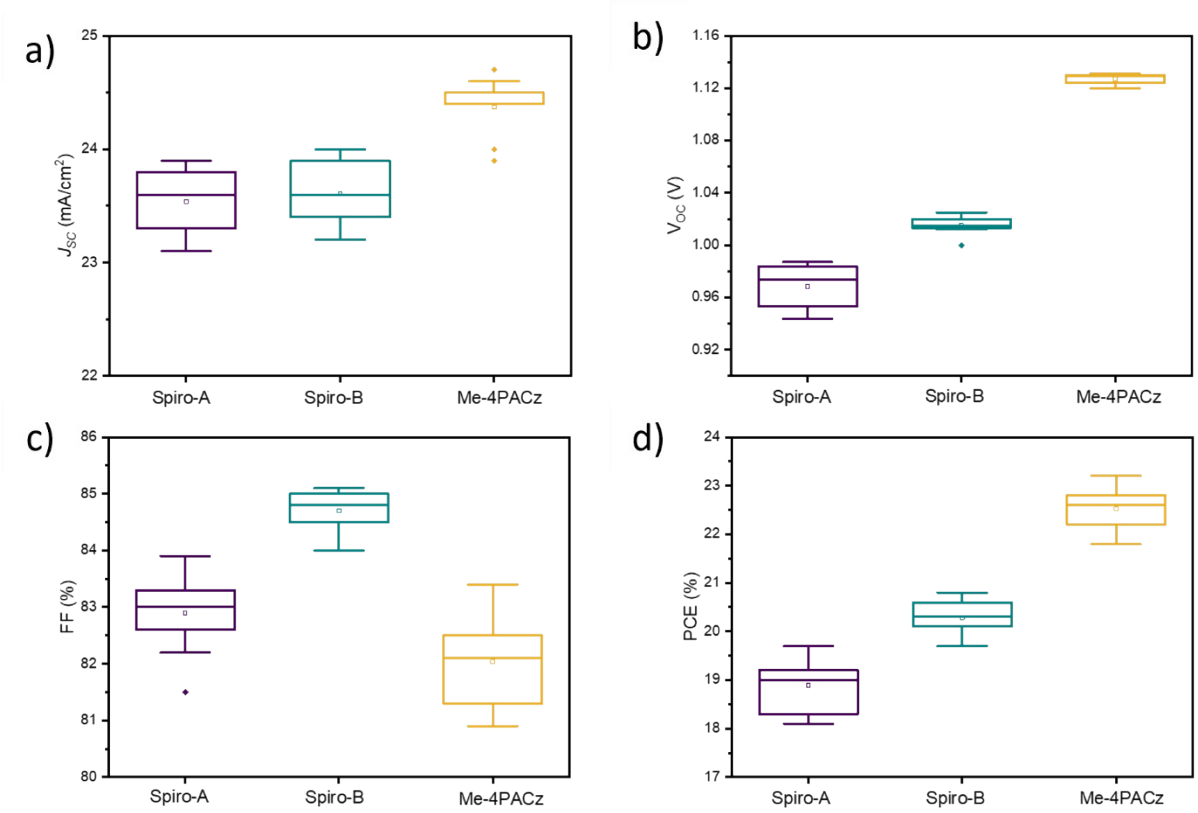

155

156 **Figure S16**. Solar cell JV parameters of **Spiro-A**, **Spiro-B** and **Me-4PACz** for a) short circuit

157 current density (mA/cm^2), b) open circuit voltage (V), c) fill factor (%) and d) power conversion

158 efficiency (PCE).

159

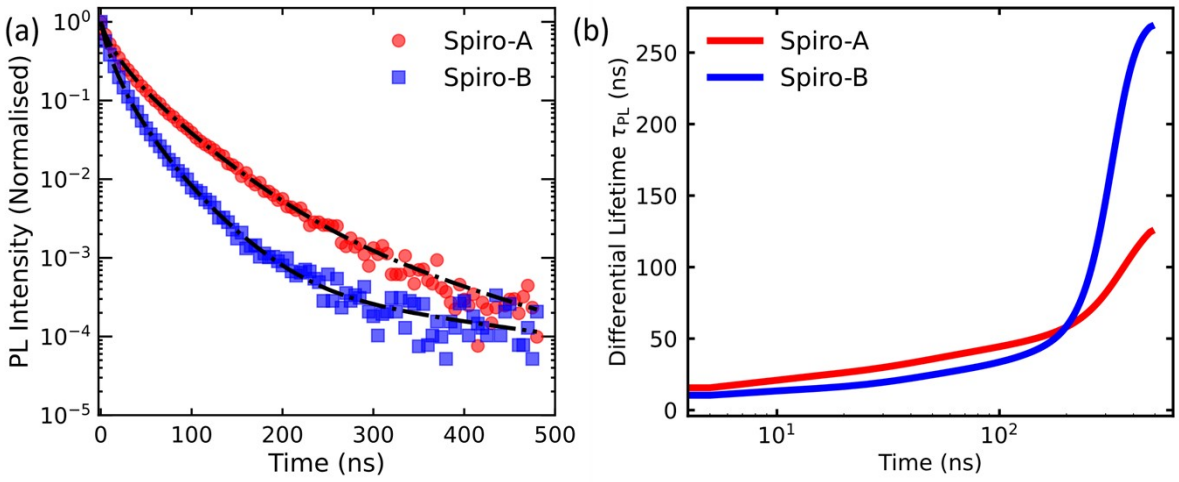

160

161 **Figure S17**. a) Normalised time-resolved photoluminescence (TRPL) data for perovskite films
162 deposited on ITO/SAM substrates. The black dashed lines represent fits made using a multi-
163 exponential decay to capture the complete dynamics. b) Differential Lifetime plots obtained from
164 the multi-exponential fits.

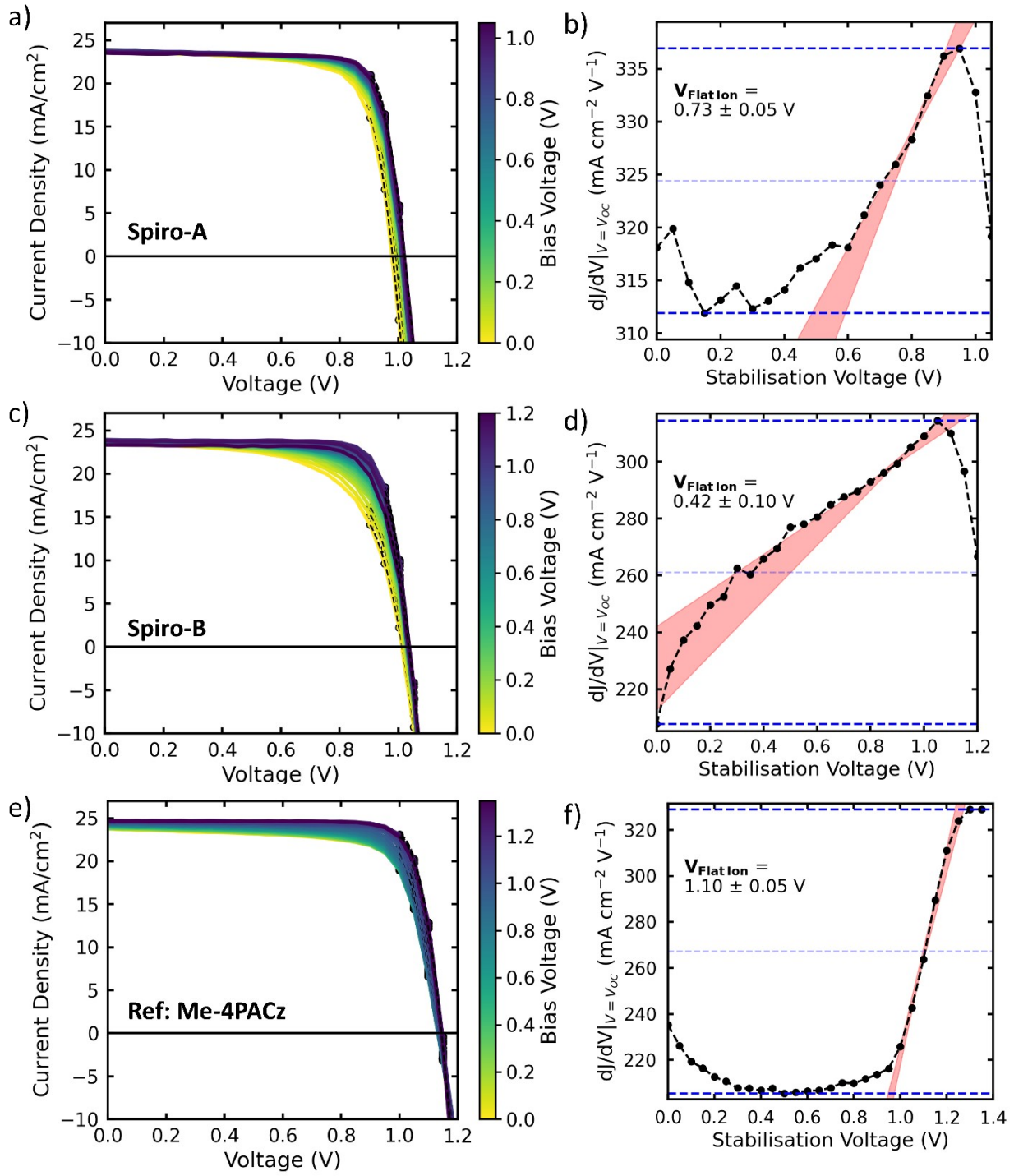

Figure S18. Full reconstructed Stabilise and Pulse JVs for a) **Spiro-A**, c) **Spiro-B** and e) **Me-4PACz** conducted under 1 Sun conditions. dJ/dV analysis for b) **Spiro-A**, d) **Spiro-B** and f) **Me-4PACz**.

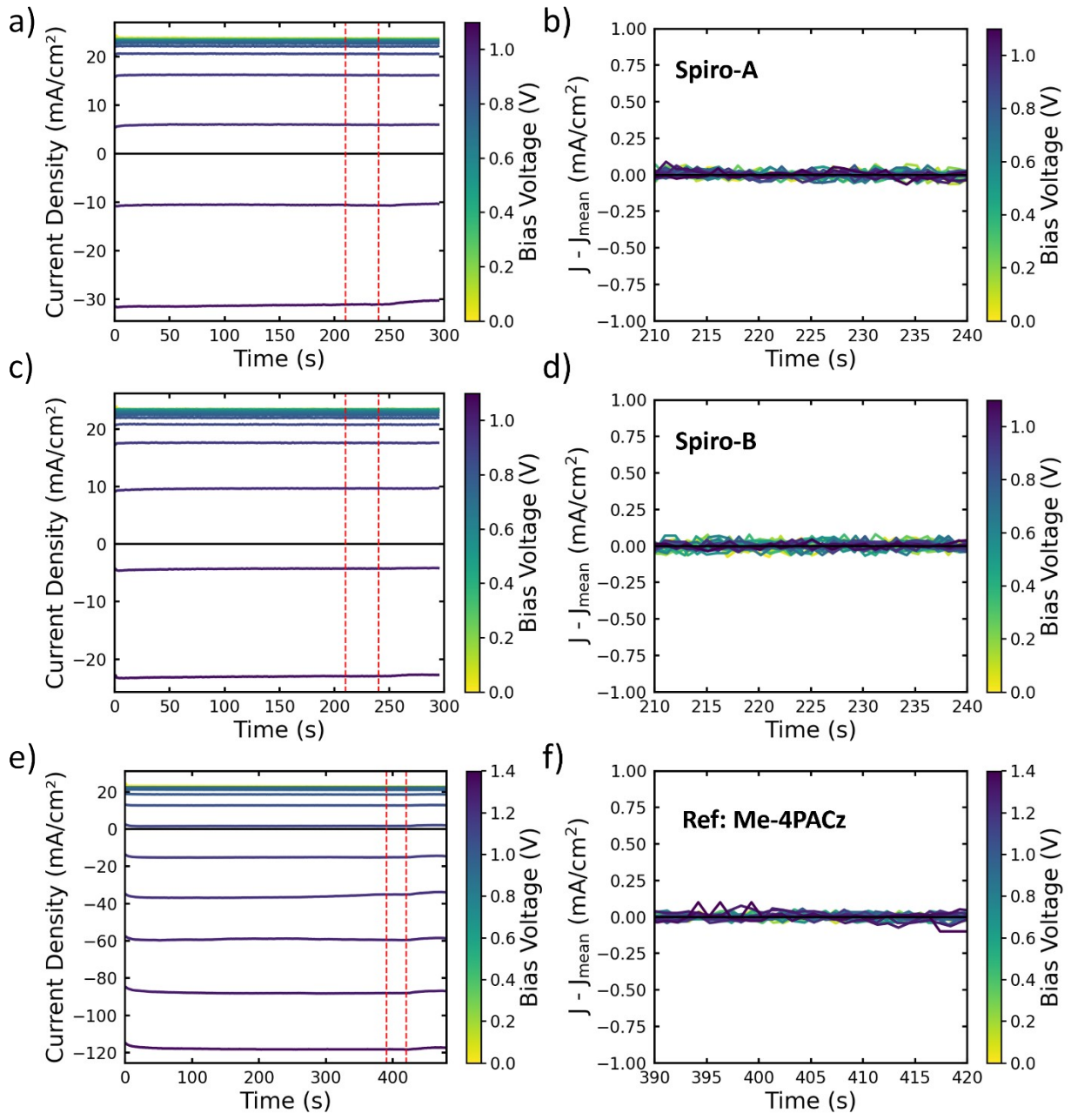

Figure S19. Full stabilisation data obtained during the Stabilise and Pulse measurement for a) **Spiro-A**, c) **Spiro-B** and e) **Me-4PACz**. Current minus the mean current for the final 30 seconds before pulsing regime for b) **Spiro-A**, d) **Spiro-B** and f) **Me-4PACz**.

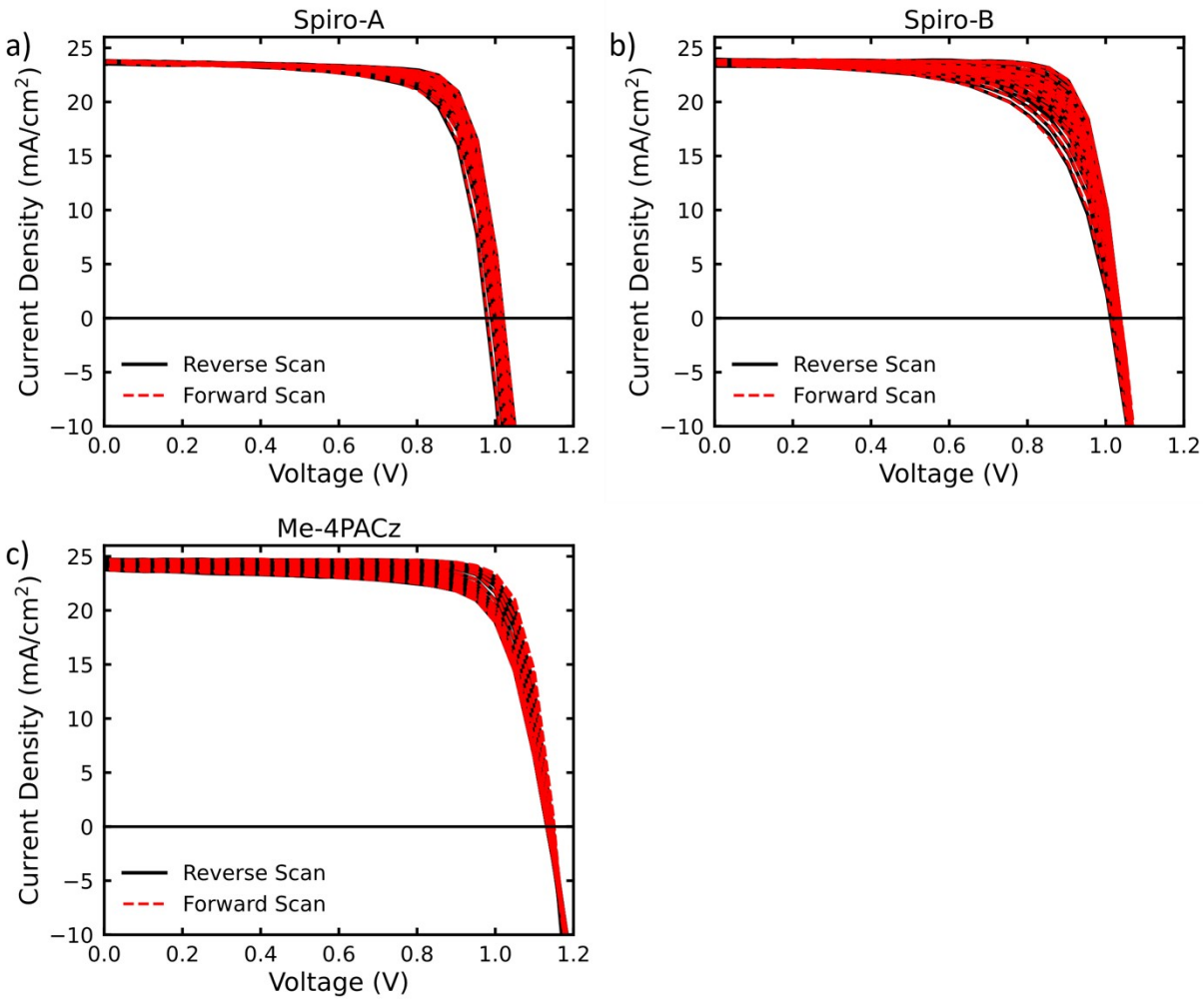

174

175 **Figure S20.** Reconstructed forward and reverse scans from the Stabilise and Pulse measurement
176 for a) **Spiro-A**, b) **Spiro-B** and c) **Me-4PACz**. Reverse scans are shown as solid black lines and
177 reverse scans as dashed red lines for a range of stabilisation voltages.

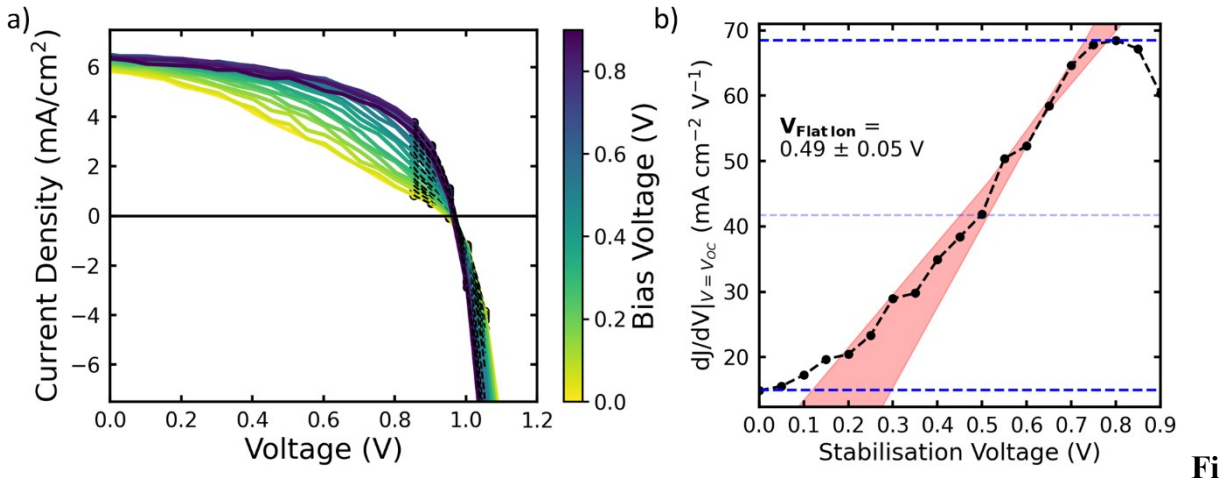

Figure S21. a) Full reconstructed low-light Stabilise and Pulse JVs for bias voltages 0-0.90 V conducted at ~0.30 Suns for **Spiro-B**. b) dJ/dV analysis of the low-light **Spiro-B** SaP.

Supplementary Tables

Material	C-C	C-N	C-O	O=C=O	C (Aro)
ITO-Ref	285.11	285.9		289.2	
Spiro Ref	284.91	285.79	286.78		291.96
Spiro-A	285.64		287.18	289.42	
Spiro-B	284.65	285.21	286.34	288.66	291.57

Material	N 1s (a)	N 1s (b)
ITO-Ref		
Spiro Ref	400.28	
Spiro-A	400.02	401.18
Spiro-B	399.82	400.38

Material	O-In	O-In-Def	HO-In	O-C
ITO-Ref	530.36	531.17	532.1	
Spiro Ref				533.52
Spiro-A	530.39	531.19	532.15	533.07
Spiro-B	530.35	530.9	531.65	533.18

Material	In 3d A	In 3d a		Sn 3d A	Sn 3d a

ITO-Ref	444.96	452.51	487.13	495.54
Spiro Ref				
Spiro-A	444.95	452.5	487.11	495.54
Spiro-B	444.9	452.45	487.04	495.46

182

183 **Table S1.** Fitted XPS Peak Positions

$\frac{dn}{dt} = -k_1 n(t) - k_2 n^2(t)$						
SAM	**k_1 (ns^{-1})**	**k_1 (%)**	**$1/k_1$ (ns)**	**k_2 (cm^3ns^{-1})**	**k_2 (%)**	**r^2**
Spiro-A	4.49×10^{-3}	28.00	222.72	3.15×10^{-19}	72.0	0.996
Spiro-B	7.52×10^{-3}	26.70	132.98	5.83×10^{-19}	73.3	0.999

Table S2. Extracted TRPL decay rate values using the rate equation for the bimolecular-trapping Auger model as shown in the first row. All measurements were conducted on half-cells using ITO/SAM/Perovskite. In the rate equation, k_1 is monomolecular recombination, k_2 is the rate of bimolecular recombination, n is the photoexcited carrier concentration, and t is time.

References

1. Z. Zeng, *et al., J. Control. Release,* 2019*,* **315**, 206–213.

2. M. J. Frisch, G. W. Trucks, H. B. Schlegel, G. E. Scuseria, M. A. Robb, J. R. Cheeseman, G. Scalmani, V. Barone, B. Mennucci, G. A. Petersson *et al.*, Gaussian 09, Revision D.01, Gaussian, Inc., Wallingford CT, 2013.